BIOCHEMISTRY
including biophysical chemistry & molecular biology

Article

pubs.acs.org/biochemistry

A Structure–Activity Analysis for Probing the Mechanism of Processive Double-Stranded DNA Digestion by λ Exonuclease Trimers

Xinlei Pan,[†,‡] Christopher E. Smith,[†,‡] Jinjin Zhang,[†,‡,⊥] Kimberly A. McCabe,[‡,@] Jun Fu,[∥] and Charles E. Bell*[,†,‡,§]

[†]Ohio State Biochemistry Program, [‡]Department of Biological Chemistry and Pharmacology, and [§]Department of Chemistry and Biochemistry, The Ohio State University, Columbus, Ohio 43210, United States

[∥]Shandong University-Helmholtz Institute of Biotechnology, State Key Laboratory of Microbial Technology, School of Life Science, Shandong University, Shanda Nanlu 27, 250100 Jinan, People's Republic of China

Supporting Information

ABSTRACT: λ exonuclease (λexo) is an ATP-independent 5′-to-3′ exonuclease that binds to double-stranded DNA (dsDNA) ends and processively digests the 5′-strand into mononucleotides. The crystal structure of λexo revealed that the enzyme forms a ring-shaped homotrimer with a central funnel-shaped channel for tracking along the DNA. On the basis of this structure, it was proposed that dsDNA enters the open end of the channel, the 5′-strand is digested at one of the three active sites, and the 3′-strand passes through the narrow end of the channel to emerge out the back. This model was largely confirmed by the structure of the λexo–DNA complex, which further revealed that the enzyme unwinds the DNA by 2 bp prior to cleavage, to thread the 5′-end of the DNA into the active site. On the basis of this structure, an "electrostatic ratchet" model was proposed, in which the enzyme uses a hydrophobic wedge to insert into the base pairs to unwind the DNA, a two-metal mechanism for nucleotide hydrolysis, a positively charged pocket to bind to the terminal 5′-phosphate generated after each round of cleavage, and an arginine residue (Arg-45) to bind to the minor groove of the downstream end of the DNA. To test this model, in this study we have determined the effects of 11 structure-based mutations in λexo on DNA binding and exonuclease activities *in vitro*, and on DNA recombination *in vivo*. The results are largely consistent with the model for the mechanism that was proposed on the basis of the structure and provide new insights into the roles of particular residues of the protein in promoting the reaction. In particular, a key role for Arg-45 in DNA binding is revealed.

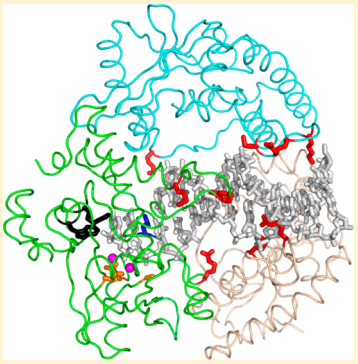

λ exonuclease (λexo) (M_r = 25.9 kDa; 226 amino acids) is a Mg^{2+}-dependent exonuclease found in bacteriophage λ.[1,2] Encoded by the *redα* gene, the enzyme is one of two key components of the Red*αβ* recombination system.[3,4] λexo binds to dsDNA ends and processively digests the 5′-strand into mononucleotides, while its partner, Red*β*, assembles on the resulting 3′-single-stranded DNA (ssDNA) overhang to anneal it to a complementary strand of a homologous duplex.[5,6] λexo and Red*β* bind to one another to form a complex known as a "synaptasome", which may serve in part to load Red*β* directly onto the 3-overhang as it is generated by λexo.[7,8] Related two-component "SynExo" recombination systems are found in a wide variety of bacteriophage, and in cryptic prophage of bacterial genomes.[9,10] Because of the high efficiency and simplicity of the single-strand annealing reactions they promote, these recombination systems have been employed in powerful new methods for genetic engineering known as "recombineering".[11−15] The λexo enzyme by itself has been employed in several other biotechnology applications, such as the Chip-Exo method for high-resolution mapping of protein–DNA binding sites,[16] and in several novel biosensors.[17−27]

The crystal structure of λexo revealed that it forms a ring-shaped homotrimer with a central funnel-shaped channel for tracking along the DNA.[28] The channel is wide enough at one end to accommodate dsDNA but narrows at the other to only allow passage of ssDNA. On the basis of this structure, a model was proposed in which dsDNA enters the open end of the channel, the 5′-strand is digested at one of the three active sites, and the 3′-strand passes through the narrow end of the channel to emerge out the back. In this way, the trimer remains topologically linked to the DNA substrate, resulting in the high degree of processivity that is observed.

Our previous structure of λexo in complex with DNA and Mg^{2+} revealed that the DNA binds to the central channel of the trimer in more or less the expected manner and is thus largely consistent with the model that was proposed (Figures 1A and 2).[29] However, the structure revealed several additional features, some of which were unexpected. First, the enzyme

Received: June 25, 2015
Revised: September 9, 2015
Published: September 11, 2015

DOI: 10.1021/acs.biochem.5b00707
Biochemistry 2015, 54, 6139–6148

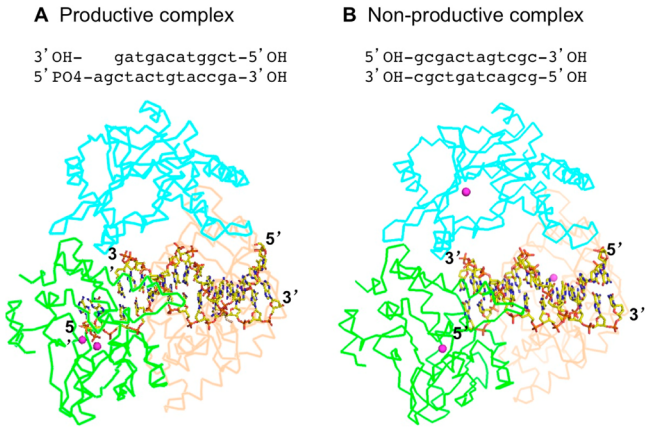

Figure 1. Crystal structures of λexo determined in complex with two different DNA substrates.[29] (A) Productive binding mode formed in complex with a 5′-phosphorylated 14-mer/12-mer DNA (PDB entry 3SM4). Notice that the two-nucleotide overhang (with 5′-phosphate) inserts into the active site of the green subunit (subunit B). (B) Nonproductive binding mode formed on a blunt-ended 12-mer duplex with a 5′-OH at both ends (PDB entry 3SLP). Notice that the DNA is bound in the central channel exactly as in panel A, except that the 5′-end of the DNA is not inserted fully into the active site. The magenta spheres show two Mg^{2+} ions in the green subunit in panel A, and a single Ca^{2+} ion (at site A) in each of the three active sites in panel B. The structure in panel A used the inactive K131A variant for the cocrystal, while the structure in panel B used the WT enzyme.

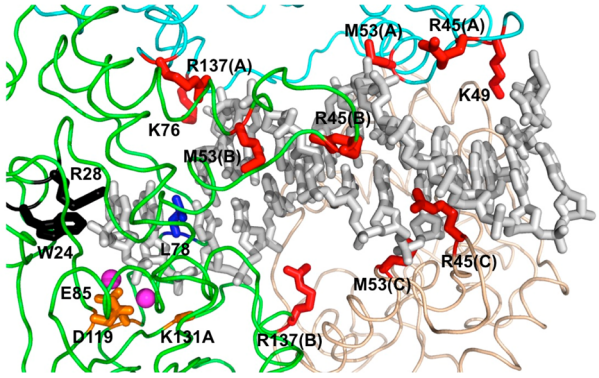

Figure 2. Locations of the 11 residues of λexo that were mutated to alanine in this study. The side chains of the mutated residues are mapped onto the crystal structure of the K131A variant of λexo determined in complex with a 5′-phosphorylated 14-mer/12-mer DNA substrate (PDB entry 3SM4).[29] The 11 residues were divided into four groups on the basis of their location in the structure: central channel (red), active site (orange), positively charged pocket (black), and hydrophobic wedge (blue). The three different subunits of the λexo trimer are colored cyan (subunit A), green (subunit B), and wheat (subunit C). The side chains of Met-53 and Arg-45 are shown for all three subunits, as these residues contact the DNA in multiple different ways. Similarly, the side chain of Arg-137 is shown for subunits A and B. The side chain of Arg-45 of subunit C, which inserts into the minor groove, makes the most intimate contact with the DNA.

unwinds exactly 2 bp from the end of the DNA prior to cleavage, such that two nucleotides from the 5′-strand twist away from the duplex to insert into one of the three active sites. Unwinding of the DNA is facilitated by a hydrophobic wedge on the protein consisting of three apolar residues, most notably Leu-78, that insert into the base pairs at the single-stranded–double-stranded junction (Figure 2). The scissile phosphate of the 5′-strand is closely bound by two Mg^{2+} ions, in a manner consistent with the two-metal mechanism proposed for MutH and other type II restriction endonuclease family enzymes.[30−33] The terminal 5′-phosphate of the DNA binds to a positively charged pocket at the end of the active site cleft formed by Arg-28, Trp-24, and several backbone amide and hydroxyl groups.[29,34] At the downstream end of the DNA, away from the active site, the DNA is bound in the central channel by a rather loose set of electrostatic interactions (Figure 2), as expected for a non-sequence-specific exonuclease. A prominent interaction is the insertion of Arg-45 into the minor groove of the DNA to form favorable electrostatic interactions, in a manner seen in the nucleosome and in other DNA binding proteins.[35,36]

The structure described above used a 12 bp duplex with a 5′-phosphorylated two-nucleotide overhang at one end, which was designed to direct the binding of λexo to that end. In the same study, the structure of λexo bound to a different DNA, a fully symmetric, blunt-ended 12-mer with a 5′-OH, was also determined (Figure 1B). In this structure, the DNA was bound in the central channel in exactly the same way as described above, but it was not unwound and inserted into the active site. This structure thus represented a nonproductive binding mode but was nonetheless important because it offered an explanation for why a 5′-phosphate group on the DNA is strictly required for activity.[1,37] This requirement had been perplexing, because even very slow cleavage of the first nucleotide of a 5′-OH substrate would leave a 5′-phosphate on the next nucleotide, because λexo generates a 5′-phosphate and 3′-OH as products. The second structure demonstrated that without a 5′-phosphate, the DNA does not even enter the active site to be cleaved in the first place, which thus highlighted the critical role of the interaction of the 5′-phosphate with the positively charged pocket, to provide the binding energy needed to unwind the DNA and initiate digestion.[29,34]

On the basis of these structures, we proposed an "electrostatic ratchet" mechanism for processivity, in which the binding of the 5′-phosphate generated after each round of cleavage to the positively charged pocket at the end of the active site provides a force to move the enzyme forward along the DNA during the reaction.[29] In addition, the insertion of Leu-78 between the bases of nucleotides 2 and 3 of the 5′-strand may act as a lever, like the pawl of a ratchet, to restrict backward movement of the enzyme along the DNA. Finally, insertion of Arg-45 into the minor groove of the downstream end of the DNA my act as a rudder, to help keep the enzyme on track as it moves along the DNA. To test this model, 11 residues of the protein that form key interactions in the structure were previously mutated to alanine, and the effects of the mutations on exonuclease activity were determined, but only qualitatively.[29]

In this study, we have extended the previous mutational analysis by measuring the effects of the 11 mutations on (1) exonuclease activity in a quantitative assay, (2) DNA binding affinity by gel-shift and fluorescence anisotropy, and (3) dsDNA recombination *in vivo*. The results are largely consistent with the electrostatic ratchet model we have proposed but reveal new insights into the precise roles of the 11 residues, as will be discussed.

EXPERIMENTAL PROCEDURES

Protein Expression and Purification. WT and mutant versions of λexo were expressed and purified as described

DOI: 10.1021/acs.biochem.5b00707
Biochemistry 2015, 54, 6139−6148

previously.[29] Briefly, the proteins were expressed in *Escherichia coli* BL21-AI cells as N-terminal six-His-tag fusions and purified by Ni affinity chromatography, thrombin cleavage to remove the six-His tag, a reverse Ni column to remove any uncleaved protein, and anion exchange on Hi-Trap QFF (GE Healthcare). Purified proteins were dialyzed into 20 mM Tris (pH 7.5) and 1 mM dithiothreitol (DTT), concentrated to >15 mg/mL, and stored at −80 °C in 100 μL aliquots.

Exonuclease Assay. The exonuclease activities of WT and mutant versions of λexo were compared using a gel-based method as described previously.[29,38] Briefly, 1 nM ^{32}P 3′-end-labeled 2.7 kB linear pUC19 DNA substrate was incubated with the indicated concentration of λexo in buffer containing 67 mM glycine-KOH (pH 9.4), 2.5 mM $MgCl_2$, and 50 mg/mL bovine serum albumin (BSA). At each time point, a 10 μL aliquot was removed from the reaction mixture, the reaction quenched with 1 μL of 0.25 mM EDTA, and the aliquot loaded onto a 0.8% agarose gel, which resolved the dsDNA substrate and ssDNA product into distinct bands. The gel was dried and autoradiographed using a Storm phosphorimager, and band intensities were quantified using ImageQuant. The rate of digestion in nucleotides per second per trimer of λexo was determined from the slope of the linear portion of the reaction (percent digestion vs time) as described previously.[38] Three independent experiments were performed for each protein (WT and 11 mutants), from which the average and standard deviation of the rate of digestion are reported in Table 2.

Gel-Shift DNA Binding Assay. A gel-shift assay to compare the binding of WT and mutant versions of λexo to a 5′-phosphorylated 14-mer/12-mer DNA duplex (Figure 1A) was performed as described previously.[38] Briefly, each 10 μL DNA binding reaction mixture contained 1 μL of 50000 cpm DNA substrate (approximately 3 nM molecules), varying concentrations of λexo (0.3−60 μM), 20 mM Tris (pH 7.5), 10 mM $CaCl_2$, and 1 mM DTT. The reaction mixtures were incubated at 25 °C for 10 min, mixed with loading dye (20% glycerol, 0.12% bromophenol blue, and 0.12% xylene cyanol), and analyzed by nondenaturing 12% PAGE in TBE buffer. Gels were dried and autoradiographed using a Storm phosphorimager, and the percentage of DNA bound was calculated as

$$\%\ \text{DNA bound} = I_C/(I_C + I_F) \times 100\%$$

where I_F and I_C are the intensities of the bands for the free and bound DNA probe, respectively. The % DNA bound was plotted against the concentration of λexo monomer and fit to the Hill equation:

$$f(x) = b + (m - b)\{1/[1 + (K_D/x)^n]\} \quad (1)$$

to obtain a value for the apparent dissociation constant (K_D), where b and m are the minimum and maximum percent of DNA bound, respectively, and n is an indication of the degree of cooperativity. We use the apparent K_D because the simplified binding model does not define explicit terms for the binding of individual monomers in the potential multistep process. For each protein, binding curves were generated from three independent experiments, from which the mean and standard deviation of the apparent K_D are reported in Table 2.

Fluorescence Anisotropy DNA Binding Assay. Fluorescence anisotropy was used to compare the binding of WT and mutant versions of λexo to a 5′-fluorescein-labeled 25 bp DNA duplex, as described previously for RecE exonuclease.[39] Briefly, 10 nM fluorescein-labeled DNA was incubated with varying concentrations of WT or mutant λexo for 20 min at 25 °C in buffer containing 20 mM Tris (pH 7.5), 10 mM $CaCl_2$, and 1 mM DTT. The fluorescence anisotropy (excitation at 490 nm, emission at 515 nm) of each 20 μL sample was measured in triplicate in Corning 384 well round-bottom black polystyrene plates using a Spectra Max M5Microplate Reader (Molecular Devices). The mean fluorescence anisotropy was plotted as a function of the concentration of λexo monomer and fit to eq 1 to obtain the apparent dissociation constant (K_D). For each protein, binding curves were generated from three independent experiments, from which the mean and standard deviation of the apparent K_D are reported in Table 2.

***In Vivo* DNA Recombination Assay.** The activities of WT and mutant versions of λexo for *in vivo* recombination were compared using a dsDNA recombineering assay established by Francis Stewart and colleagues.[40,41] The Redα, Redβ, and Redγ functions were expressed from an arabinose-inducible, temperature-sensitive pSC101-BAD-gba-tet (no *recA*) plasmid in *E. coli* GB2005 (*recA*−) cells. The 12 Redα mutations were introduced into the pSC101 plasmid using the QuikChange method (Stratagene) and confirmed by DNA sequencing. Each pSC101 plasmid was co-electroporated into GB2005 cells together with the p15A plasmid that is one of the substrates for the recombination assay, and colonies were selected at 30 °C on LB-agar plates containing 10 μg/mL chloramphenicol (p15A) and 4 μg/mL tetracycline (pSC101); 1.2 mL overnight cultures were grown in triplicate from single colonies in LB with antibiotics using a 24-tube Eppendorf thermomixer at 30 °C and 1000 rpm. Overnight cultures were diluted to a starting OD of 0.1 in 1.2 mL of fresh LB with antibiotics and grown for 2 h at 30 °C to an OD of ∼0.6. Ten microliters of 20% arabinose was added to induce expression of the Redαβγ proteins, and cells were grown for an additional 40 min at 37 °C. Cells were placed immediately on ice, centrifuged at 1000 rpm and 4 °C in an Eppendorf microcentrifuge, and resuspended in 1 mL of ice-cold 10% glycerol. This step was repeated twice, and the final pelleted cells were resuspended in ∼50 μL of 10% glycerol and placed on ice. Two microliters of 50 ng/μL linear dsDNA neomycin polymerase chain reaction (PCR) product was added, and the mixture was transferred to a 1 mm electroporation cuvette (MidSci EC1) and shocked at 1.45 V using a Bio-Rad *E. coli* pulser. One milliliter of LB medium was added to each electroporation cuvette, and the cells were transferred to a 1.5 mL microcentrifuge tube, shaken at 900 rpm for 1 h at 37 °C, and plated at an appropriate volume on an LB-agar plate with 15 μg/mL kanamycin and 10 μg/mL chloramphenicol. After overnight incubation at 37 °C, the number of colonies on each plate was counted. Experiments for each mutant were performed in triplicate, and the average and standard deviation of the number of colonies per final milliliter of culture are reported in Table 2.

Western Blots. For each of the 11 pSC101 plasmids containing a different Redα mutation, normal expression of λexo and Redβ proteins under the conditions of the assay was confirmed by Western blotting. Cell lysates expressing λexo mutants were prepared according to a modified recombineering protocol. Briefly, GB2005 cells containing the appropriate pSC101 plasmid were grown in LB at 30 °C to an OD_{600} of ∼0.3 and induced with 0.2% arabinose for 40 min at 37 °C. Soluble lysate samples were run on 13.5% SDS−PAGE and then transferred to a nitrocellulose membrane (Bio-Rad) for 80 min at 20 V (constant voltage) and 4 °C. Membranes were blocked with 1% BSA in PBST (phosphate-buffered saline with 0.5% Tween) for 1 h at room temperature and then incubated

DOI: 10.1021/acs.biochem.5b00707
Biochemistry 2015, 54, 6139−6148

with anti-Red$\alpha\beta$ antibody for 1.5 h at room temperature in PBST with 1% BSA to probe for λexo and Redβ proteins. Membranes were then incubated with horseradish peroxidase-conjugated goat anti-rabbit antibody for 1 h at 25 °C in PBST with 1% BSA. Chemiluminescence was detected using Super-Signal West Pico Chemiluminescent Substrate (Thermo Scientific) and visualized on X-ray film.

RESULTS

Design of the Mutations. The 11 mutant versions of λexo were designed and prepared as has been described, on the basis of the crystal structure of the λexo−DNA complex.[29] The positions of the mutated residues in the structure of λexo are shown in Figure 2, and the contacts they make with the DNA are listed in Table 1. Five of the mutations (R45A, K49A, M53A, K76A, and R137A) were introduced at residues of the protein that line the central channel to contact the downstream portion of the DNA, away from the active site. One of the mutations, L78A, is at a key residue of the hydrophobic wedge that inserts into the base pairs of the DNA to unwind it.

Three of the mutations (K131A, D119A, and E85A) were introduced at highly conserved active site residues. Two of the mutations (W24A and R28A) are at residues of the positively charged pocket that binds to the 5′-phosphate. It is important to note that because the complex is formed by a protein trimer bound to a single DNA duplex, a given residue of the protein could in principle contact the DNA in multiple (up to three) different ways, depending on the subunit (A, B, or C). This is indeed the case for many of the residues that line the central channel, but not for the residues of the hydrophobic wedge, the active site, or the site for binding the 5′-phosphate (Figure 2).

Our previous qualitative comparison of the exonuclease activities of these λexo variants ranked them in order of decreasing activity as WT, M53A, K76A, K49A, L78A, W24A, and E85A.[29] No activity was observed for R45A, R28A, R137A, K131A, and D119A. The goals of this study were to determine the exonuclease activities of these λexo variants quantitatively and to determine the effects of the mutations on DNA binding and on recombination *in vivo*.

Exonuclease Activity. Our previous method for examining the exonuclease activity used agarose gel electrophoresis with SYBR Gold fluorescent stain to monitor digestion of a linear 2.7 kb pUC19 dsDNA substrate under conditions of limiting enzyme.[29] Because of the processive nature of the reaction, in which one strand of the duplex is cleaved into mononucleotides to release the opposing strand intact, this method allows for simultaneous visualization of the dsDNA substrate and ssDNA product. However, we found that the SYBR Gold stain was not quantitative, because the signal for the DNA did not vary linearly with concentration. Therefore, as described in detail elsewhere,[38] we used a ^{32}P 3′-end-label to visualize the DNA and confirmed that the signal for the DNA varied linearly with concentration. The 3′-end of the DNA was labeled instead of the 5′-end because λexo is a 5′−3′ exonuclease. Exonuclease assays were performed at pH 9.4, the optimal pH for the reaction,[42] which presumably facilitates deprotonation of the active site Lys-131 residue.[29]

Raw data for the ^{32}P-based exonuclease assay are shown in Figure 3 for WT λexo and three of the variants and in Figure S1 for all of the variants. The measured rates of digestion, determined from three independent experiments for each protein, are reported in nucleotides per second in Table 2. The rate measured for WT by this method is 41 ± 4 nucleotides/s, which is reasonably close to values ranging from 3 to 32 nucleotides/s determined either biochemically[1,34,37] or in four single-molecule studies.[43−46] Dramatically higher rates (~1000 nucleotides/s) have been measured in other single-molecule studies,[47−51] for reasons that are not yet clear. Three of the variants, K49A, K76A, and M53A, retained at least 37% of the activity of WT λexo. All three of these mutations are at residues of the central channel that make predominantly loose

Table 1. List of Atomic Contacts between Mutated Residues and the DNA Substrate, As Seen in the Crystal Structure of the Complex (PDB entry 3SM4)[29,a]

		(A) Central Channel		
Arg-45(A)	NH1	Ade-10(E)	OP2	3.37
Arg-45(B)	NH2	Ade-8(D)	OP1	2.75
Arg-45(C)	NH1	Cyt-11(E)	O2	3.20
	NH1	Thy-5(D)	O2	3.51
	NH2	Ade-6(D)	O4′	3.69
	NH2	Cyt-11(E)	O3′	4.34
Lys-49(A)	NZ	Gua-3(D)	OP2	4.89
	NZ	Cyt-2(D)	OP2	4.03
Lys-49(B)	NZ	Gua-9(D)	OP1	9.17
Lys-49(C)	NZ	Cyt-7(D)	OP2	7.87
	NZ	Ade-6(D)	OP1	6.79
Met-53(A)	CE	Gua-8(E)	C5′	3.87
	SD	Gua-8(E)	C3′	3.91
Met-53(B)	SD	Ade-8(D)	C2′	3.69
	SD	Gua-9(D)	C8	3.84
	CE	Thy-10(D)	C7	3.59
Met-53(C)	SD	Thy-5(D)	C5′	4.33
	SD	Thy-5(D)	C3′	4.42
Lys-76(A)	NZ	Gua-12(D)	OP2	2.61
Lys-76(B)	NZ	Ade-5(E)	OP2	5.72
Lys-76(C)	NZ	Cyt-6(E)	OP1	6.42
	NZ	Thy-7(E)	OP1	7.40
Arg-137(A)	NH2	Ade-11(D)	OP1	2.85
	NH1	Ade-11(D)	OP2	2.99
Arg-137(B)	NH2	Ade-5(E)	OP2	4.48
	NH2	Thy-4(E)	OP1	4.94
Arg-137(C)	NH1	Thy-7(E)	OP1	5.58
	NH1	Gua-8(E)	OP2	6.54
		(B) Hydrophobic Wedge		
Leu-78(B)	CD2	Cyt-3(E)	N3	3.39
	CD1	Gua-2(E)	C2	3.68
	CB	Gua-2(E)	N3	3.56
		(C) Active Site		
Glu-85(B)	OE1	Gua-2(E)	OP1	4.05
Asp-119(B)	OD2	Gua-2(E)	OP1	3.13
	OD2	Gua-2(E)	OP1	3.13
Lys-131(B)	NZ	Gua-2(E)	OP2	3.46*
		(D) 5′-Phosphate		
Trp-24(B)	CH2	Ade-1(E)	C4	4.18
	CZ3	Ade-1(E)	C2	4.40
Arg-28(B)	NH1	Ade-1(E)	OP2	3.30
	NH1	Ade-1(E)	OP3	3.38

[a]The numbers in the right column give the distances (in angstroms) between the specified atoms of the protein (left) and DNA (middle). Chain E of the DNA is the strand with its 5′-end bound in the active site of subunit B of the protein. The distance for Lys-131 (indicated by the asterisk) is taken from a composite model of the complex described previously,[52] because the 3SM4 structure used the K131A variant. A schematic view of these interactions can be found in supplementary Figure S3 of ref 29.

DOI: 10.1021/acs.biochem.5b00707
Biochemistry 2015, 54, 6139−6148

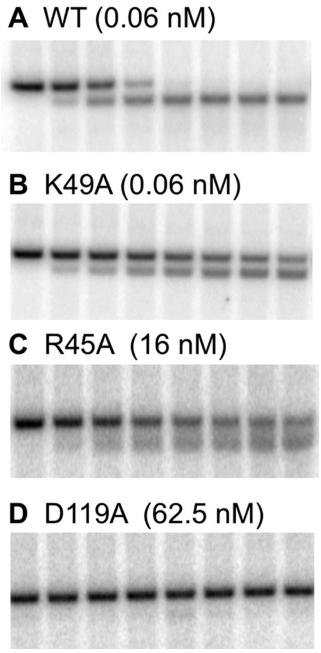

Figure 3. Gel-based exonuclease assay for WT λexo and three variants. Each agarose gel shows a time course for the reaction of (A) WT or (B–D) mutant λexo with 1 nM ^{32}P 3′-end-labeled linear 2686 bp pUC19 dsDNA. The upper band of each gel is the dsDNA substrate, and the lower band is the ssDNA product. Time points from left to right are 0, 5, 10, 15, 20, 25, 30, and 40 min, respectively. The concentration of enzyme added to each experiment (expressed as nanomolar trimer) is indicated above each gel image. Higher concentrations of enzyme were used for the mutants with lower activity, so that changes in band intensities could be accurately measured on the same time scale. The figure compares WT (full activity) with mutants that have slightly lower activity (K49A), barely detectable activity (R45A), and no detectable activity (D119A).

electrostatic or van der Waals contacts with the DNA. The L78A mutation, which is the central residue of the hydrophobic wedge, results in a more significant reduction in activity, to 12% of that of the WT.

Four of the mutations, E85A, R45A, R137A, and W24A, result in a level of activity that is detectable, but drastically lowered, to less than 2% of that of the WT. Two of these residues, Arg-45 and Arg-137, line the central channel to contact the downstream end of the DNA. Arg-45 of subunit C, which we will call Arg-45(C), makes the most intimate contact with the downstream end of the DNA, where its guanidinium group inserts into the minor groove, midway between the two sugar–phosphate backbones (Figure 2). The side chains of Arg-45(A) and Arg-45(B) also interact closely with the DNA, forming ion pairs (within 3.4 Å) with backbone phosphates (Table 1). The Arg-137 residue of all three subunits is within 6 Å of the DNA. Arg-137(A) makes a particularly strong bidentate ion pair with one of the phosphates of the 3′-strand, near where it would exit the central channel (Figure 2). Arg-137(B) and Arg-137(C) make longer range (4.5–5.6 Å) electrostatic contacts with phosphates of the 5′-strand. Glu-85 is a highly conserved residue of the active site that is ∼5 Å from the scissile phosphate and the two active site Mg^{2+} ions. Glu-85 does not directly coordinate either of the two Mg^{2+} ions, or the scissile phosphate, and may play a more indirect role in catalysis, such as in fine-tuning the electrostatics, or possibly interacting with a water molecule that protonates the 3′-oxyanion leaving group. Such roles would be consistent with the E85A variant retaining a level of activity detectable but significantly lower than that of the WT. Finally, Trp-24 is located at the end of the active site cleft, where one edge of its indole ring packs against the face of the base of the terminal 5′-nucleotide, and the other edge is directed toward the 5′-phosphate.

Table 2. Exonuclease Activity, DNA Binding Affinity, and *in Vivo* Recombination Activity Measured for WT λexo and 11 Mutants[a]

	(A) apparent K_D (μM) by EMSA (5′-PO_4)	(B) Hill coefficient by EMSA (5′-PO_4)	(C) K_D (nM) by FA (5′-PO_4)	(D) Hill coefficient by FA (5′-PO_4)	(E) K_D (nM) by FA (5′-OH)	(F) Hill coefficient by FA (5′-OH)	(G) K_{cat} (nucleotides/s)	(H) *in vivo* recombination, no. of colonies (×10^3 mL^{-1})
WT	2.1 ± 0.3	2.5 ± 0.7	112 ± 9	6 ± 3	93 ± 3	5.2 ± 1.4	41 ± 4	32 ± 9
K49A	16.8 ± 0.5	2.1 ± 0.3	180 ± 20	2.6 ± 0.4	130 ± 30	1.5 ± 0.2	19 ± 2	6.6 ± 1.1
K76A	3.5 ± 0.8	3.2 ± 0.4	148 ± 8	5.8 ± 0.8	90 ± 4	3.0 ± 0.3	15 ± 2	7.9 ± 1.4
M53A	3.9 ± 0.6	3.5 ± 1.4	118 ± 6	4.3 ± 0.3	87 ± 2	2.7 ± 0.4	29 ± 1	13 ± 3
R45A	172 ± 17	1.6 ± 0.2	3600 ± 400	0.8 ± 0.1	4600 ± 1100	0.8 ± 0.2	0.100 ± 0.003	3.5 ± 1.3
R137A	12 ± 7	3.0 ± 0.8	253 ± 8	1.6 ± 0.3	210 ± 24	1.4 ± 0.1	0.30 ± 0.02	1.3 ± 0.5
L78A	2.3 ± 0.4	3.4 ± 0.2	112 ± 13	5.2 ± 1.8	108 ± 19	2.6 ± 0.8	5 ± 3	4.4 ± 1.5
D119A	2.9 ± 1.2	3.2 ± 0.9	125 ± 2	3.6 ± 0.3	93 ± 1	2.6 ± 0.2	0	3.3 ± 0.9
E85A	3.7 ± 0.9	2.7 ± 1.5	127 ± 6	8 ± 2	81 ± 9	3.2 ± 0.5	0.7 ± 0.3	2.5 ± 0.3
K131A	4.9 ± 1.4	4.0 ± 0.5	187 ± 8	3.3 ± 0.2	141 ± 32	1.9 ± 0.4	0	0.20 ± 0.05
R28A	5.3 ± 1.1	4.9 ± 0.3	101 ± 6	8.6 ± 1.3	105 ± 21	3.3 ± 0.8	0	2.3 ± 1.2
W24A	2.6 ± 0.3	4.3 ± 0.9	122 ± 9	7 ± 3	117 ± 18	5.1 ± 1.6	–	2.2 ± 1.0
R45K	2.0 ± 0.3	2.5 ± 0.4					40 ± 5	26 ± 7
DEL								2.8 ± 0.7

[a](A and B) Apparent K_D and Hill coefficients (n) measured by EMSA with a 5′-phosphorylated 14-mer/12-mer dsDNA substrate. (C–F) Apparent K_D and Hill coefficients (n) measured by FA with a 5′-fluorescein-labeled 25-mer dsDNA substrate. For columns C and D, the DNA contained a 5′-phosphate at the opposite end from the fluorescein, while for columns E and F, this end of the DNA contained a 5′-OH. (G) *In vitro* exonuclease activity measured by the agarose gel assay, from quantitation of the gels shown in Figure 3 and Figure S1. The rate for W24A could not be calculated because the reaction appeared to be distributive (see the legend of Figure S1). (H) *In vivo* recombination activity measured by the dsDNA recombineering assay described in Experimental Procedures. The value in the table gives the number of colonies per milliliter of final cell culture. For all of the experiments, the number in the table gives the mean and standard deviation from at least three (A–G) or six (H) independent experiments.

DOI: 10.1021/acs.biochem.5b00707
Biochemistry 2015, 54, 6139–6148

Three of the mutations, K131A, D119A, and R28A, result in variants with no detectable activity, even at elevated enzyme:substrate ratios. Asp-119 is the aspartate of the DEK motif that bridges the two active site Mg^{2+} ions, and thus, the total lack of activity for this variant is expected. Lys-131 is the highly conserved lysine of the DEK motif that binds and activates the attacking water molecule. The K131A variant was used to trap the λexo−DNA complex for crystallization,[29] and thus, its total lack of activity is also expected. Arg-28 is not part of the active site but is a key residue of the positively charged pocket that binds to the 5′-phosphate group of the DNA.[29,34] The total lack of activity for R28A is consistent with a critical role for the interaction of the 5′-phosphate with this residue for catalysis. On the basis of the crystal structures, it is likely that this interaction is necessary to unwind the DNA to insert the 5′-strand into the active site for cleavage. The interaction could also be required for correct alignment of the scissile phosphate within the active site, once the DNA is unwound.

DNA Binding. The DNA binding affinities of WT and mutant λexo proteins were compared using two different methods, a gel-shift assay with the same 5′-phosphorylated 14-mer/12-mer DNA that was used in the crystal structure and fluorescence anisotropy (FA) with a 25 bp duplex containing a 5′-fluorescein at one end and a 5′-phosphate (or 5′-OH) at the other. Raw data and binding curves for the two methods are shown for the WT and selected variants in Figure 4 and for all

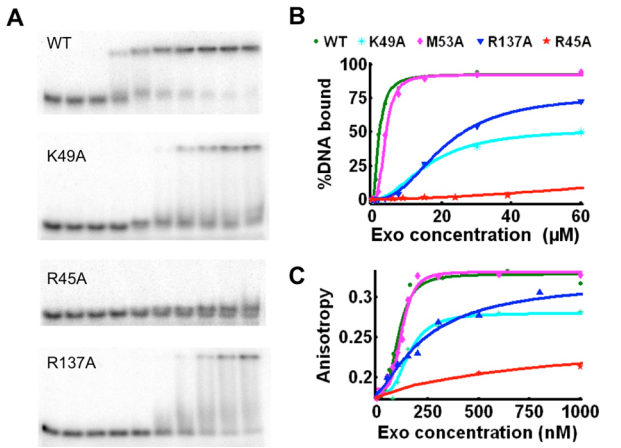

Figure 4. DNA binding assays for WT, K49A, R45A, and R137A variants of λexo. (A) Gel-shift assay with a ^{32}P 5′-end-labeled 14-mer/12-mer dsDNA substrate. The concentration of λexo monomers in each lane from left to right is 0, 0.3, 0.6, 0.9, 1.8, 3.6, 7.5, 15, 30, and 60 μM, respectively. (B) Fits of the data from the gel-shift assays. The % DNA bound was calculated from the band intensities from the gels of panel A and plotted vs the concentration of λexo monomer. The solid line shows the fit of the data to the Hill equation, as described in Experimental Procedures. (C) Fluorescence anisotropy assay. A 5′-fluorescein-labeled 25-mer dsDNA was equilibrated with varying concentrations of λexo protein, and the anisotropy was measured in triplicate as described in Experimental Procedures. The solid line shows the fit of the data to the Hill equation. Notice that R45A is the only variant with substantially diminished DNA binding affinity.

of the variants in Figures S2−S4. All DNA binding experiments were performed at pH 7.5. Although this differs from the pH of 9.4 used for the exonuclease assays, a control experiment using the FA method demonstrates similar binding affinities for WT λexo at either pH (Figure S5). The apparent K_D values determined from three independent experiments for each mutant are reported in Table 2 for each method. For all of the proteins, the affinity measured by gel shift (K_D of 2.1 ± 0.3 μM for the WT) was approximately 20−40-fold weaker than that measured by fluorescence anisotropy (K_D of 112 ± 9 nM for the WT). This may reflect tighter binding of λexo to the 25 bp duplex as compared to the 12 bp duplex, and/or weaker binding in the gel-shift assay caused by partial dissociation of the complex under the force of migration through the gel. Despite this difference, the trends seen in comparing the affinities observed for the λexo variants to one another were very similar for both methods. For both methods, the binding curves were better fit to a cooperative binding model using the Hill equation than to a noncooperative 1:1 (trimer−DNA) binding model,[39] as shown in Figure S6. This likely reflects a linkage between the equilibrium of association of λexo monomers to form a trimer and the binding of the trimer to the DNA. Thus, the apparent K_D values reported in Table 2 are based on the concentration of λexo monomer, as opposed to trimer. Values for the Hill coefficient (n) ranged from 0.8 to 8.6. In general, although the differences in the n values for the different measurements reported in Table 2 were statistically significant, the values for some of the proteins varied significantly for the different methods. Because λexo is not known to form oligomers larger than a trimer, we do not at present have a physical explanation for n values of >3. Accurate measurement of this parameter may require more data points in the transition region for some of the proteins.

The R45A mutation had by far the most significant effect on DNA binding, reducing the affinity by 82-fold in the gel-shift assay and by 32-fold in the FA assay (Table 2). Only two other mutations, K49A and R137A, decreased the binding affinity by >3-fold. The K49A variant bound to DNA with 8-fold reduced affinity as determined in the gel-shift assay and 1.6-fold reduced affinity as determined by FA, while the affinity of R137A was 6-fold weaker as determined by the gel-shift assay and 2.3-fold weaker as determined by FA. All three of these mutations occur at residues that line the central channel of the trimer to contact the downstream portion of the DNA. The dramatically decreased level of binding of the R45A variant is consistent with the prominent role of Arg-45 seen in the structure, where its guanidinium group inserts deeply into the minor groove to form favorable electrostatic interactions.[29] By contrast, the contacts involving Lys-49 and Arg-137 are in general more distant and subtle, except for those of the Arg-137 side chain of subunit A. Thus, for residues lining the central channel, the effects of the mutations on DNA binding affinity are consistent with the interactions seen in the crystal structure.

It was surprising to us, however, that mutations at many of the residues that make close contacts with the DNA elsewhere in the structure, such as W24A, L78A, R28A, K131A, and D119A, had little to no effect on the observed DNA binding affinity. This result could potentially be explained by considering the two different binding modes observed in the crystal structures (Figure 1). All of these residues contact the DNA in the productive binding mode, in which the DNA is unwound and inserted into the active site (Figure 1A), but not in the nonproductive mode, in which the DNA is only bound to the central channel (Figure 1B). If these two binding modes have similar affinities, then mutations that shift the equilibrium from one binding mode to the other would not be expected to affect the observed binding affinity significantly. Although the productive binding mode clearly has more extensive interactions, there is an energetic penalty to pay for DNA

DOI: 10.1021/acs.biochem.5b00707
Biochemistry 2015, 54, 6139−6148

unwinding. On the other hand, the nonproductive mode has fewer interactions but no penalty for unwinding. Consistent with this interpretation, all of the mutations that do cause a measurable decrease in affinity (R45A, K49A, and R137A) occur at residues of the central channel that contact the downstream portion of the DNA in both binding modes.

As a further test of this interpretation, we compared the binding of DNAs containing a 5′-OH and a 5′-phosphate on the non-fluorescein-labeled end of the 25-mer in the FA assay and found that the presence of the 5′-phosphate did not have a large effect (≤1.6-fold) on the affinity of WT or any of the λexo variants for the DNA (columns C and E of Table 2). It is likely that the absence of the 5′-phosphate, like the active site mutations, destabilizes the productive binding mode, shifting the equilibrium to the nonproductive binding mode, which has a similar affinity. Even though the 5′-phosphate is required for activity, a similar binding affinity can apparently be achieved for a nonphosphorylated DNA in the nonproductive binding mode. This conclusion is further supported by competition experiments, which demonstrated that a DNA containing a 5′-OH is able to compete off a DNA containing a 5′-phosphate, and vice versa, although the DNA with the 5′-phosphate was a slightly more potent competitor (Figure S7).

dsDNA Recombination *in Vivo*. Next, we compared the activities of WT and the 11 λexo variants for dsDNA recombineering *in vivo*. We used the method of Stewart and colleagues,[40,41] in which the Redαβγ functions are expressed (in the absence of *recA*) from a temperature-sensitive, arabinose-inducible pSC101-based plasmid in GB2005 *E. coli* cells, which are *recA*−. A 2.1 kB PCR product encoding the neomycin gene flanked by 50 bp homologies to a target site on a chloramphenicol-resistant p15A plasmid is electroporated into arabinose-induced cells containing p15A and pSC101 plasmids. Redαβγ-mediated recombination of the dsDNA PCR product into the p15A plasmid results in a colony on an LB-agar plate containing kanamycin and chloramphenicol. The 11 λexo mutations described above, as well as a deletion generated by mutating the codon for Trp-24 into a stop codon, were introduced into the pSC101 plasmid, and the expression of both the λexo and Redβ proteins from the 13 plasmids was confirmed by Western blotting (Figure 5). The recombination frequencies for WT λexo, the 11 variants, and the deletion were measured in triplicate and are reported in Table 2 as the number of colonies formed per milliliter of the final cell culture.

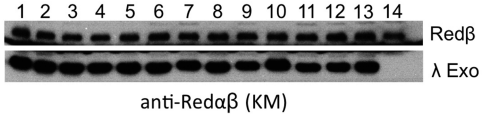

Figure 5. Western blots showing protein expression from pSC101 plasmids encoding WT and 12 mutant versions of λexo with Redβ. Cultures of *E. coli* GB2005 cells transformed with pSC101 and p15A plasmids were grown and induced under the conditions of the recombineering assay and harvested by centrifugation. Soluble portions of cell lysates prepared by sonication were run on an SDS−PAGE gel, blotted onto nitrocellulose, and reacted with the anti-Redαβ antibody as described in Experimental Procedures. Proteins in each lane are as follows: top panel, Redβ; bottom panel, lane 1, WT; lane 2, K49A; lane 3, K76A; lane 4, M53A; lane 5, R45A; lane 6, R137A; lane 7, L78A; lane 8, D119A; lane 9, E85A; lane 10, K131A; lane 11, R28A; lane 12, W24A; lane 13, R45K; lane 14, *redα* deletion construct.

The data in Table 2 are representative of several experiments for each variant performed each time in triplicate. Control experiments in the absence of arabinose, p15A plasmid, or PCR product consistently resulted in zero colonies, indicating that all of the colonies were dependent on expression of the Red recombineering functions and the presence of both of the DNA substrates.

As seen in column H of Table 2, all of the variants have significantly reduced activity for dsDNA recombination *in vivo*. Three of the variants, K49A, K76A, and M53A, retained at least 20% of the activity of the WT. These residues make predominantly subtle contacts with the DNA, and their mutation to alanine has only mild effects on the exonuclease and DNA binding activities *in vitro*. For these variants, there is a good correlation between the effects of the mutations *in vivo* and *in vitro*.

The least active variant was K131A. In fact, the recombination activity for K131A was significantly and reproducibly lower than that seen for the λexo deletion construct. This suggests that a low level of recombination is occurring in the absence of intact λexo protein (but in the presence of Redβ and Redγ), presumably because of one or more endogenous *E. coli* nucleases, and that the K131A protein is in some way inhibitory, such as by binding and blocking the DNA ends from being accessed by Redβ or other host nucleases. The recombination activities of several of the variants, D119A, E85A, R28A, R45A, R137A, and W24A, were approximately 5−10% of that of the WT, which was similar to the deletion construct, for which no intact λexo protein was present. All of these variants had little to no activity in the exonuclease assay, and thus, for these proteins, there is good correlation between the activities seen *in vitro* and *in vivo*.

R45K Mutation. Given the dramatic effect of the R45A mutation on DNA binding, it was of interest to determine if the function of this residue depends on the specific interactions of the guanidinium group, or simply on the positive charge. Thus, the R45K variant was purified and tested for exonuclease activity and DNA binding. As seen in Figure 6 and Table 2, the R45K variant maintained the full activity of the WT protein in both the exonuclease and DNA binding assays. Similarly, in the dsDNA recombination assay, the R45K variant had 82% of the activity of the WT *in vivo*, whereas R45A had only 11%, close to the background of 9% seen for the *redα* deletion (Table 2).

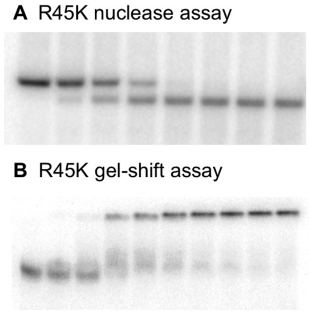

Figure 6. R45K variant has full exonuclease and DNA binding activities. (A) Exonuclease assay performed as described in the legend of Figure 3 for WT λexo. Time points from left to right are 0, 5, 10, 15, 20, 25, 30, and 40 min, respectively. (B) Gel-shift assay performed as described in the legend of Figure 4 for WT λexo. The concentration of λexo monomer in each lane is 0, 0.3, 0.6, 0.9, 1.8, 3.6, 7.5, 15, 30, and 60 μM (from left to right, respectively).

DOI: 10.1021/acs.biochem.5b00707
Biochemistry 2015, 54, 6139−6148

These results indicate that it is the positive charge of Arg45, as opposed to the specific interactions of the guanidinium group, that is important for DNA binding and exonuclease activity. Although Arg-45 of subunit C makes by far the most intimate contact with the DNA through the insertion of its guanidinium group into the minor groove, the Arg-45 side chains of the other two subunits also make close ion pairs with the phosphates (Table 1), making it difficult to sort out the relative importance of the three different interactions.

DISCUSSION

This study is to the best of our knowledge the first to systematically determine the effects of mutations on the *in vivo* activity of either of the Redα (λexo) or Redβ recombineering functions. For the most part, the effects of the mutations in λexo on *in vivo* recombination mirror their effects on exonuclease activity *in vitro*. The three mutations that have the mildest effects on exonuclease activity *in vitro*, K49A, K76A, and M53A, have among the mildest effects on recombination *in vivo*. Similarly, most of the mutations that result in very little (E85A, W24A, R137A, and R45A) or no (R28A, D119A, and K131A) exonuclease activity *in vitro* result in low levels of *in vivo* recombination that are comparable to that of the deletion construct, for which no intact λexo protein is expressed. Interestingly, the three mutations with the mildest effects overall, K49A, K76A, and M53A, result in at most a 2−3-fold reduction in exonuclease activity *in vitro*, but a more dramatic 3−5-fold reduction in recombination activity *in vivo*. We do not yet understand the basis for the stronger effect of the mutations seen *in vivo* as compared to *in vitro*.

The main difference between the effects of the individual mutations *in vitro* and *in vivo* was the very low activity of the K131A protein seen *in vivo*. K131A was the only variant for which the *in vivo* recombination activity was actually lower than that of the deletion construct. This suggests that the K131A protein inhibits *in vivo* recombination in some way, such as by binding tightly to the DNA ends to block Redβ and/or other host nuclease enzymes from gaining access. However, the K131A protein did not have increased DNA binding affinity in the gel-shift or FA assays, and its behavior in all of the *in vitro* assays was similar to that of D119A and R28A, two mutants that did not exhibit an inhibitory effect *in vivo*. Thus, the basis for the unique inhibitory effect of K131A *in vivo* is not explained by the data presented here.

As discussed above, the observation that mutations at many of the residues that form close contacts with the DNA in the crystal structure do not affect DNA binding affinity can potentially be explained if there are multiple DNA binding modes, such as the two seen in the crystal structures. A DNA substrate that λexo would encounter *in vivo* would typically have a 5′-phosphate, which would tend to favor the productive DNA binding mode. Whether or not the two different binding modes are important mechanistically remains to be determined, but the nonproductive binding mode could conceivably be important for the initial recognition and capture of a DNA substrate. This could be tested if a mutation that specifically disrupts the nonproductive binding mode could be isolated. However, because all of the residues that contact the DNA in the nonproductive binding mode also contact the DNA in the productive binding mode, design of such a mutant would be difficult. Whether or not the protein uses a two-step mechanism for DNA binding, with the nonproductive mode occurring first, followed by a transition to the productive mode, could conceivably be tested *in vitro* by techniques such as time-resolved fluorescence quenching. For example, Trp-24 contacts the DNA in the productive binding mode, but not in the nonproductive mode. Such experiments are beyond the scope of this work but could be the subject of future studies.

The results of the experiments reported here generally support the "electrostatic ratchet" model for the mechanism of λexo that we proposed previously on the basis of the crystal structure[29] but further clarify the roles of individual residues in DNA binding and catalysis. Two of the key residues of the electrostatic ratchet mechanism are Arg-28 and Leu-78. Arg-28 is a residue of the positively charged pocket that binds to the 5′-phosphate, while Leu-78 forms the "pawl" of the ratchet that inserts into the base pairs of the DNA to potentially restrict backward movement. The results of this study indicate that Arg-28 is much more critical for λexo activity than is Leu-78. R28A was completely inactive *in vitro* and gave only background levels of activity *in vivo*. By contrast, the L78A variant maintains a significant level of activity *in vitro*, ∼12% of that of the WT, and approximately twice the recombination activity of R28A (and the deletion construct) *in vivo*. These results suggest that while the "electrostatic" part of the mechanism is a critical feature, the "ratchet" part of the model is not. It should be noted, however, that the mutation of a leucine to an alanine is a more conservative substitution than an arginine to an alanine mutation, as the alanine maintains some of the hydrophobic character of the leucine. Moreover, Leu-78 is only one of three residues, the other two being Val-73 and Ala-75, that wedge into the base pairs to form hydrophobic interactions to unwind the DNA. Nonetheless, the new data show that while Arg-28 is critical for activity, Leu-78 is not.

The data reported here suggest a critical role for Arg45. Arg45 forms a prominent interaction with the downstream portion of the DNA substrate, where its guanidinium group inserts into the minor groove to form favorable electrostatic interactions. On the basis of this interaction, we had proposed that Arg-45 may act as a "rudder", to help keep the enzyme on track as it moves along the DNA. Arginine residues that form similar minor groove interactions in other proteins have been shown to be critical for DNA binding.[36] Moreover, this type of interaction can also be used for sequence-specific DNA recognition, as the arginine insertion prefers AT-rich regions for which the minor groove is narrowed.[35,36] The observation that the R45K mutant maintains the DNA binding and exonuclease activities of the WT protein implies that it is the positive charge at this position that is important, as opposed to specific interactions or properties of the planar guanidinium group. In addition to Arg-45 of subunit C that wedges into the minor groove, the Arg-45 residues of subunits A and B also contact the DNA, through close ion pairs with phosphates. A lysine could in principle form these latter two interactions nearly as well as an arginine, which is consistent with the observation that the R45K mutant is active. On the basis of these results, it appears that it is the positive charge at this residue position, potentially in all three subunits, that is important for DNA binding affinity, as opposed to the insertion of the guanidinium group into the minor groove that occurs only in subunit C. Thus, the idea that Arg-45 may act as a rudder to keep the enzyme on track is not supported by these data. Arg-137, another positively charged residue that contacts the DNA in all three subunits, is just as important as Arg-45 for *in vitro* exonuclease activity and *in vivo* recombination, but less important for DNA binding affinity. Collectively, the

DOI: 10.1021/acs.biochem.5b00707
Biochemistry 2015, 54, 6139−6148

interactions that the three Arg-137 residues make with the DNA are not as intimate as those of Arg-45 (Table 1), but it appears that the positive charge at this position is just as important for function.

CONCLUSION

This work is the first to compare the effects of mutations in λexo on the activity of the protein *in vitro* and *in vivo*. As expected, the results reveal a critical role for three highly conserved active site residues Lys-131, Asp-119, and Glu-85. The results reveal an equally critical role for Arg-28, a residue of the positively charged pocket that binds to the 5′-phosphate of the DNA. This electrostatic interaction may be important for providing a directional force for movement of the enzyme along the DNA after each round of cleavage. The results reveal a less critical role for Leu78, a residue of the hydrophobic wedge that inserts into the base pairs to unwind the DNA. Finally, the results reveal a critical role of Arg45 for DNA binding affinity and exonuclease activity *in vitro* and *in vivo*, although it is the positive charge at this residue position that is important, as opposed to specific features of the guanidinium group.

ASSOCIATED CONTENT

Supporting Information

The Supporting Information is available free of charge on the ACS Publications website at DOI: 10.1021/acs.biochem.5b00707.

Raw data for each protein variant for the exonuclease and DNA binding assays, a control experiment showing that the binding affinity of λexo for DNA is the same at pH 7.5 and 9.5, and competition experiments showing that the DNA with a 5′-OH competes off DNA with a 5′-phosphate, and vice versa (PDF)

AUTHOR INFORMATION

Corresponding Author

*E-mail: bell.489@osu.edu. Telephone: 614-688-3115.

Present Addresses

⊥J.Z.: Infectious Disease Division, NewLink Genetics Corp., 2503 South Loop Dr., Suite 5100, Ames, IA 50010.

@K.A.M.: Department of Anthropology, Northwestern University, Evanston, IL 60208.

Author Contributions

X.P. and C.E.S. contributed equally to this work.

Funding

This work was funded by Grant MCB-1021966 (to C.E.B.) from the National Science Foundation.

Notes

The authors declare no competing financial interest.

ACKNOWLEDGMENTS

We thank Dr. Francis Stewart for providing extensive advice, materials, and protocols for the dsDNA recombineering experiments. We thank Dr. Donald Court and Dr. Lynn Thomason for providing the anti-Redαβ antibodies used for the Western blot of Figure 5, which they had originally obtained from Dr. Kenan Murphy. We thank Dr. Lynn Thomason and Dr. Gohkan Tolun for comments on the manuscript.

ABBREVIATIONS

λexo, λ exonuclease; dsDNA, double-stranded DNA; ssDNA, single-stranded DNA; SDS−PAGE, sodium dodecyl sulfate−polyacrylamide gel electrophoresis; EDTA, ethylenediaminetetraacetic acid; TAE, tris-acetate-EDTA; TBE, tris-borate-EDTA; FA, fluorescence anisotropy; BSA, bovine serum albumin; PBST, phosphate-buffered saline with 0.5% TWEEN; OD, optical density; DTT, dithiothreitol; WT, wild type; PDB, Protein Data Bank.

REFERENCES

(1) Little, J. W. (1967) An exonuclease induced by bacteriophage lambda II. Nature of the enzymatic reaction. *J. Biol. Chem. 242*, 679−686.

(2) Carter, D. M., and Radding, C. M. (1971) The role of exonuclease and β protein of phage λ in genetic recombination. II. Substrate specificity and the mode of action of λ exonuclease. *J. Biol. Chem. 246*, 2502−2512.

(3) Kuzminov, A. (1999) Recombinational repair of DNA damage in *Escherichia coli* and bacteriophage lambda. *Microbiol. Mol. Biol. Rev. 63*, 751−813.

(4) Stahl, M. M., Thomason, L., Poteete, A. R., Tarkowski, T., Kuzminov, A., and Stahl, F. W. (1997) Annealing *vs.* invasion in phage λ recombination. *Genetics 147*, 961−977.

(5) Muniyappa, K., and Radding, C. M. (1986) The homologous recombination system of phage lambda. Pairing activities of beta protein. *J. Biol. Chem. 261*, 7472−7478.

(6) Kmiec, E., and Holloman, W. K. (1981) Beta protein of bacteriophage lambda promotes renaturation of DNA. *J. Biol. Chem. 256*, 12636−12639.

(7) Radding, C. M., Rosenzweig, J., Richards, F., and Cassuto, E. (1971) Separation and characterization of exonuclease, β protein, and a complex of both. *J. Biol. Chem. 246*, 2510−2512.

(8) Muyrers, J. P., Zhang, Y., Buchholz, F., and Stewart, A. F. (2000) RecE/RecT and Redα/Redβ initiate double-stranded break repair by specifically interacting with their respective partners. *Genes Dev. 14*, 1971−1982.

(9) Datta, S., Costantino, N., Zhou, X., and Court, D. L. (2008) Identification and analysis of recombineering functions from Gram-negative and Gram-positive bacteria and their phages. *Proc. Natl. Acad. Sci. U. S. A. 105*, 1626−1631.

(10) Vellani, T. S., and Myers, R. S. (2003) Bacteriophage SPP1 Chu is an alkaline exonuclease in the SynExo family of viral two-component recombinases. *J. Bacteriol. 185*, 2465−2474.

(11) Poteete, A. R. (2001) What makes the bacteriophage lambda Red system useful for genetic engineering: molecular mechanism and biological function. *FEMS Microbiol. Lett. 201*, 9−14.

(12) Zhang, Y., Buchholz, F., Muyrers, J. P., and Stewart, A. F. (1998) A new logic for DNA engineering using recombination in *Escherichia coli*. *Nat. Genet. 20*, 123−128.

(13) Copeland, N. G., Jenkins, N. A., and Court, D. L. (2001) Recombineering: a powerful new tool for mouse functional genomics. *Nat. Rev. Genet. 2*, 769−779.

(14) Sharan, S. K., Thomason, L. C., Kuznetsov, S. G., and Court, D. L. (2009) Recombineering: a homologous recombination-based method of genetic engineering. *Nat. Protoc. 4*, 206−223.

(15) Wang, H. H., Isaacs, F. J., Carr, P. A., Sun, Z. Z., Xu, G., Forest, C. R., and Church, G. M. (2009) Programming cells by multiplex genome engineering and accelerated evolution. *Nature 460*, 894−898.

(16) Rhee, H. S., and Pugh, B. F. (2011) Comprehensive genome-wide protein-DNA interactions detected at single-nucleotide resolution. *Cell 147*, 1408−1419.

(17) Gerasimova, Y. V., and Kolpashchikov, D. M. (2014) Enzyme-assisted target recycling (EATR) for nucleic acid detection. *Chem. Soc. Rev. 43*, 6405−6438.

DOI: 10.1021/acs.biochem.5b00707
Biochemistry 2015, 54, 6139−6148

(18) Liu, L., Lei, J., Gao, F., and Ju, H. (2013) A DNA machine for sensitive and homogeneous DNA detection via lambda exonuclease assisted amplification. *Talanta 115*, 819−822.
(19) Zhang, J., Tao, M., and Jin, Y. (2014) An enzyme-aided amplification strategy for sensitive detection of DNA utilizing graphene oxide (GO) as a fluorescence quencher. *Analyst 139*, 3455−3459.
(20) Schweighardt, A. J., Battaglia, A., and Wallace, M. M. (2014) Detection of anthrax and other pathogens using a unique liquid array technology. *J. Forensic Sci. 59*, 15−33.
(21) Duan, R., Zuo, X., Wang, S., Quan, X., Chen, D., Chen, Z., Jiang, L., Fan, C., and Xia, F. (2014) Quadratic isothermal amplification for the detection of microRNA. *Nat. Protoc. 9*, 597−607.
(22) Yuan, Z., Zhou, Y., Gao, S., Cheng, Y., and Li, Z. (2014) Homogenous and sensitive detection of microRNA with ligase chain reaction and lambda exonuclease-assisted cationic conjugated polymer biosensing. *ACS Appl. Mater. Interfaces 6*, 6181−6185.
(23) Ge, J., Tang, L. J., Xi, Q., Li, X. P., Yu, R. Q., Jiang, J. H., and Chu, X. (2014) A WS2 nanosheet based sensing platform for highly sensitive detection of T4 polynucleotide kinase and its inhibitors. *Nanoscale 6*, 6866−6872.
(24) Hou, T., Wang, X., Liu, X., Lu, T., Liu, S., and Li, F. (2014) Amplified detection of T4 polynucleotide kinase activity by the coupled λ exonuclease cleavage reaction and catalytic assembly of molecular beacons. *Anal. Chem. 86*, 884−890.
(25) Miao, P., Ning, L., Li, X., Shu, Y., and Li, G. (2011) An electrochemical alkaline phosphatase biosensor fabricated with two DNA probes coupled with λ exonuclease. *Biosens. Bioelectron. 27*, 178−182.
(26) Wang, L., Liu, Y., and Li, J. (2014) Self-phosphorylating deoxyribozyme initiated cascade enzymatic amplification for guanosine-5′-triphosphate detection. *Anal. Chem. 86*, 7907−7912.
(27) Wang, Y., Chen, J., Jiao, H., Chen, Y., Li, W., Zhang, Q., and Yu, C. (2013) Polymer-templated perylene-probe noncovalent self-assembly: a new strategy for label-free ultrasenstive fluorescence turn-on biosensing. *Chem. - Eur. J. 19*, 12846−12852.
(28) Kovall, R., and Matthews, B. W. (1997) Toroidal structure of lambda-exonuclease. *Science 277*, 1824−1827.
(29) Zhang, J., McCabe, K. A., and Bell, C. E. (2011) Crystal structures of lambda exonuclease in complex with DNA suggest an electrostatic ratchet mechanism for processivity. *Proc. Natl. Acad. Sci. U. S. A. 108*, 11872−11877.
(30) Kovall, R. A., and Matthews, B. W. (1999) Type II restriction endonucleases: structural, functional, and evolutionary relationships. *Curr. Opin. Chem. Biol. 3*, 578−583.
(31) Pingoud, A., Fuxreiter, M., Pingoud, V., and Wende, W. (2005) Type II restriction endonucleases: structure and mechanism. *Cell. Mol. Life Sci. 62*, 685−707.
(32) Lee, J. Y., Chang, J., Joseph, N., Ghirlando, R., Rao, D. N., and Yang, W. (2005) MutH complexed with hemi- and unmethylated DNAs: coupling base recognition and DNA cleavage. *Mol. Cell 20*, 155−166.
(33) Yang, W., Lee, J. Y., and Nowotny, M. (2006) Making and breaking nucleic acids: Two-Mg^{2+}-ion catalysis and substrate specificity. *Mol. Cell 22*, 5−13.
(34) Subramanian, K., Rutvisuttinunt, W., Scott, W., and Myers, R. S. (2003) The enzymatic basis of processivity in lambda exonuclease. *Nucleic Acids Res. 31*, 1585−1596.
(35) West, S. M., Rohs, R., Mann, R. S., and Honig, B. (2010) Electrostatic interactions between arginines and the minor groove in the nucleosome. *J. Biomol. Struct. Dyn. 27*, 861−866.
(36) Rohs, R., West, S. M., Sosinsky, A., Liu, P., Mann, R. S., and Honig, B. (2009) The role of DNA shape in protein-DNA recognition. *Nature 461*, 1248−1253.
(37) Mitsis, P. G., and Kwagh, J. G. (1999) Characterization of the interaction of lambda exonuclease with the ends of DNA. *Nucleic Acids Res. 27*, 3057−3063.
(38) Pan, X., Yan, J., Patel, A., Wysocki, V. H., and Bell, C. E. (2015) Mutant poisoning demonstrates a nonsequential mechanism for digestion of double-stranded DNA by λ exonuclease trimers. *Biochemistry 54*, 942−951.
(39) Zhang, J., Xing, X., Herr, A. B., and Bell, C. E. (2009) Crystal structure of *E. coli* RecE protein reveals a toroidal tetramer for processing double-stranded DNA breaks. *Structure 17*, 690−702.
(40) Wang, J., Sarov, M., Rientjes, J., Fu, J., Hollak, H., Kranz, H., Xie, W., Stewart, A. F., and Zhang, Y. (2006) An improved recombineering approach by adding RecA to lambda red recombination. *Mol. Biotechnol. 32*, 43−54.
(41) Fu, J., Bian, X., Hu, S., Wang, H., Huang, F., Seibert, P. M., Plaza, A., Xia, L., Müller, R., Stewart, A. F., and Zhang, Y. (2012) Full-length RecE enhances linear-linear homologous recombination and facilitates direct cloning for bioprospecting. *Nat. Biotechnol. 30*, 440−446.
(42) Little, J. W., Lehman, I. R., and Kaiser, A. D. (1967) An exonuclease induced by bacteriophage λ I. Preparation of the crystalline enzyme. *J. Biol. Chem. 242*, 672−678.
(43) Dapprich, J. (1999) Single-molecule DNA digestion by lambda-exonuclease. *Cytometry 36*, 163−168.
(44) Van Oijen, A. M., Blainey, P. C., Crampton, D. J., Richardson, C. C., Ellenberger, T., and Xie, X. S. (2003) Single-molecule kinetics of λ exonuclease reveal a base dependence and dynamic disorder. *Science 301*, 1235−1238.
(45) Perkins, T. T., Dalal, R. V., Mitsis, P. G., and Block, S. M. (2003) Sequence-dependent pausing of single lambda exonuclease molecules. *Science 301*, 1914−1918.
(46) Lee, G., Yoo, J., Leslie, B. J., and Ha, T. (2011) Single-molecule analysis reveals three phases of DNA degradation by an exonuclease. *Nat. Chem. Biol. 7*, 367−374.
(47) Matsuura, S., Komatsu, J., Hirano, K., Yasuda, H., Takashima, K., Katsura, S., and Mizuno, A. (2001) Real-time observation of a single DNA digestion by λ exonuclease under a fluorescence microscope field. *Nucleic Acids Res. 29*, E79.
(48) Oliver-Calixte, N. J., Uba, F. I., Battle, K. N., Weerakoon-Ratnayake, K. M., and Soper, R. A. (2014) Immobilization of lambda exonuclease onto polymer micropillar arrays for solid-phase digestion of dsDNAs. *Anal. Chem. 86*, 4447−4454.
(49) Kang, S. H., Lee, S., and Yeung, E. S. (2010) Digestion of individual DNA molecules by λ-exonuclease at liquid-solid interface. *Analyst 135*, 1759−1764.
(50) Lee, S., Kang, S. H., and Yeung, E. S. (2011) Enzyme digestion of entrapped single-DNA molecules in nanopores. *Talanta 85*, 2135−2141.
(51) Lee, S., and Kang, S. H. (2013) Single-molecule DNA digestion in various alkanethiol-functionalized gold nanopores. *Talanta 107*, 297−303.
(52) Zhang, J., Pan, X., and Bell, C. E. (2014)) Crystal structure of λ exonuclease in complex with DNA and Ca(2+). *Biochemistry 53*, 7415−7425.

DOI: 10.1021/acs.biochem.5b00707
Biochemistry 2015, 54, 6139−6148